Minor and trace element emissions from post-combustion CO₂ capture from coal: Experimental and equilibrium calculations

A. Cotton, K. Patchigolla *, J.E. Oakey

Centre for Energy and Resource Technology, Cranfield University, Cranfield MK43 0AL, UK

HIGHLIGHTS

- Tested pilot scale, 25 kWth CO₂ capture reactor, using Ca-based CO₂ sorbent.
- Flue gas trace element emission sampling based on EPA Method 29.
- EDS analysis undertaken of Ca-based sorbent for elemental analysis.
- Sensitivity analysis carried out on MTDATA software, for 9 and 21 trace elements.
- Thermodynamic equilibrium modelling undertaken to support experimental work.

ARTICLE INFO

ABSTRACT

Elemental partitioning, including gaseous elemental emissions from pilot scale (25 kWth), post combustion CO₂ capture using a Ca-based sorbent, have been investigated for naturally occurring elemental impurities found in limestone, that have the potential to be released to the environment under carbonation and calcination conditions. Inductively Coupled Plasma-Mass Spectrometry (ICP-MS) analysis of Longcliffe SP52 limestone was undertaken to identify other impurities present, and the effect of sorbent mass and SO₂ concentration on elemental partitioning in the carbonator between solid sorbent and gaseous phase was investigated, using a bubbler sampling system. Samples were analysed using ICP-MS, which showed that sorbent mass and SO₂ concentration in the carbonator effected the concentrations of gaseous trace elements sampled. Thermodynamic modelling of the carbonation and calcination process was also undertaken, based on molar quantities of trace elements identified from ICP-MS analysis of limestone, which provided useful information with regards to element stability and partitioning under realistic CO₂ capture conditions.

© 2013 Elsevier Ltd. All rights reserved.

1. Introduction

Calcium looping is a method of CO₂ capture which utilises fluidised bed technology, whereby a particulate bed is fluidised using a gas within a reactor. In this case the particulate bed comprises a limestone-derived CO₂ sorbent, and the fluidising gas comprises CO₂-containing flue gas. The calcium looping cycle makes use of the reversible carbonation reaction, and the subsequent CO₂ capture and release process is therefore cyclic. The equilibrium carbonation–calcination reaction is provided by Eq. (1), whereby carbonation is exothermic and calcination is endothermic. The reactors for carbonation (carbonator) and calcination (calciner) are separate, meaning that there is no gaseous exchange between the two, ensuring the efficiency of the process is optimised.

$$CaO + CO_2 \leftrightarrow CaCO_3 \qquad \Delta H^\circ_r = \pm 178 \text{ kJ mol}^{-1} \qquad (1)$$
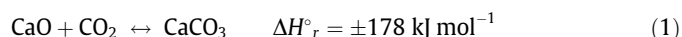
The use of limestone as a CO₂ sorbent in fluidised bed carbon capture systems from coal, is gaining attention due to the high availability, low cost, and potential for high CO₂ sorption efficiency of Ca based sorbents. However, limestone is a naturally-occurring material, and always contains other species in the form of trace elements. The high temperature conditions under which carbonation and calcination occur, present opportunities for trace elements to be released to the environment, thereby representing a potential source of environmental contamination, in addition to that produced from coal combustion. A large amount of research has been carried out on the use of limestone in the calcium looping cycle as a method of CO₂ capture, but to date only minimal work has been carried out on the potential pollutants that may be produced by the calcium looping cycle as a result of limestone impurities.

Environmental and human health problems can arise from emissions of toxic heavy metals, with Pb, As, Hg, Cd, Cr and Zn of

* Corresponding author. Tel.: +44 (0)1234 750111; fax: +44 (0)1234 750875.
E-mail address: k.patchigolla@cranfield.ac.uk (K. Patchigolla).

particular cause for concern. In addition, the presence of such trace elements may cause technical uncertainties within energy production systems, including corrosion of construction materials [1,2].

Several studies have shown that trace elements released from coal during energy processes tend to partition either between gaseous emissions, or ash residues, dependant on their volatility. Based on this partitioning tendency, it has been suggested that trace elements can be classed into three main groups [3–5]:

- Group I elements – least volatile, partition into ash residues e.g. Mn, Be, Co, Cr.
- Group II elements – moderate volatility, partition between ash residues and gaseous phase. As gases cool, vapour species condense onto particulate matter e.g. As, Cd, Pb, Sb.
- Group III elements – High volatility and unlikely to condense from vapour phase e.g., Hg, and Se.

Group III and Group II elements are considered to represent the greatest risk to the environment and human health due to their increased volatility compared to Group I elements. These groups describe element behaviour, and therefore are considered valid regardless of the process in question.

Córdoba et al. [6] investigated the partitioning of elements in a pulverised coal combustion power plant fitted with wet limestone flue gas desulphurisation (FGD). The most volatile elements including S and F were retained by the FGD-derived gypsum, whilst moderately volatile elements including As and B were for the most part retained in the fly ash. Gaseous emissions were below European directive 2001/80/EC limits for large combustion plants and the pollutant release and transfer register (Pollutant Release and Transfer Registry (PRTR)) threshold values, with the exception of Hg emissions and particulate Se, As, Zn, Cu, Ni, and Cr.

The fate of trace elements was investigated in a 90 kW oxy-combustion pilot plant fed with coal and limestone [7]. It was shown that 82% of elemental Hg was emitted in the exhaust gas, as was 81% of Cl. It was further suggested that the relatively low temperatures, and high Ca content in the system from limestone use promoted condensation and sorption of sulphate, fluoride and chloride species.

Meij [4] analysed the concentrations and distributions of trace elements within coal-fired power plants fitted with FGD technology, employing limestone as an SO_2 sorbent. It was found that the predominant source of trace elements within the FGD plants were from limestone, suggesting that the use of limestone-derived CO_2 sorbents may represent a further potential source of trace elements within power stations, and in turn may impact on downstream processes. Further, Sager [8] also suggests that lime used for gas scrubbing within a power plant may introduce trace elements to the system, including As, Pb, Cd and Zn.

By contrast, Furimsky [9] concluded that limestone sorption of trace elements may have a diluting effect on trace element content in coal ash, whilst Cheng et al. [10] suggested lime (CaO) may be beneficial in reducing trace element emissions from coal combustion. Metal oxides other than $CaCO_3$ have been identified in limestone, including MgO, Al_2O_3, SiO_2 and Fe_2O_3, in addition to trace elements [11,12] whilst Barber [13] concluded that Ca, Mg, Mn and Sr are mainly restricted to the carbonate fraction of limestone, and that 'mineralogical associations' of trace elements in limestone are complex.

With regards to elemental emissions from limestone use during the calcium looping cycle for CO_2 capture, Dean [14] carried out experiments at the bench scale to investigate the effect of coal use on limestone-derived sorbent trace element inventory. Experiments carried out without coal use showed no change in sorbent trace element inventory. Batch experiments carried out using La Jagua coal showed an increase in the concentration of Ba, Cr, K, Mn, Sr, and Ti, whilst concentrations of B, Na and K remain the same, whilst for Cu there was a small decrease. For continuous experiments comparing 2 different coals and refuse-derived fuel (RDF), an increase in Al content was observed suggesting some ash mixed in with the sorbent. The concentrations of Ba, K, Sr and Zn remained the same for all fuels. For Lea Hall coal, there was an increase in B over eight cycles from ~20 to 40 ppm, though not for La Jagua. For Cu, sorbent concentrations in the first cycle (~15 ppm) remained the same over eight cycles for the two coals, but increased over five cycles in the presence of RDF from ~20 ppm to ~180 ppm. Na remained the same for the sorbent cycled in the presence of La Jagua, but there was an increase in results for Lea Hall coal and RDF from ~250 to ~550 ppm and from ~200 to 400 ppm respectively, expected given that the Na content of the La Jagua coal is an order of magnitude lower than of the other two fuels. Ti remained the same for La Jagua over eight cycles, though saw an increase in the sorbent cycled in the presence of RDF over five cycles from ~50 ppm to ~150 ppm. There appear to be no further studies available in the literature investigating elemental partitioning as a result of limestone use in the calcium looping cycle.

Several studies within the literature make use of thermodynamic equilibrium modelling software in predicting trace element release during energy production. Thompson and Argent [15,16] have used thermodynamic equilibrium modelling to investigate trace element mobilisation under both combustion and air-blown gasification conditions. One of the most widely used software packages, Metallurgical and Thermodynamic Databank (MTDATA), designed and produced by the National Physical Laboratory (NPL), UK, has been used to investigate trace element release including during combustion of wood bark [17], combustion of sewage sludge with Polish coal [18], in investigating trace element release from biomass-fuelled gasification systems [19], and in investigating trace element, including mercury, emissions from gasification and combustion conditions [20]. Goni et al. [21] utilised MTDATA to model fusibility during combustion of different coal blends, and confirmed that the equilibrium calculations were a valid tool in doing so. Khodier et al. [1] used MTDATA to model the combustion and deposition process when co-firing miscanthus with coal, and concluded it a useful predictive tool to support experimental analytical techniques. With regards to CCS in particular, MTDATA has been used to predict the impact of impurities on CO_2 transport in relation to the pipeline transport of dense phase CO_2 from a capture plant to a subsurface storage site [22], but otherwise, it can be concluded that there is limited data available in the literature with regards to using thermodynamic modelling to support experimentally-derived trace element emissions results from CO_2 capture.

This objective of this study was to experimentally investigate the elemental partitioning between solid sorbent and gaseous release from the use of limestone-derived CO_2 sorbent, within a 25 kWth pilot scale CO_2 capture reactor. In order to support the experimental study, MTDATA has been used here to investigate the likely compounds to be formed under realistic reaction conditions, and also to examine the stability of those compounds under typical Ca looping conditions.

2. Experimental procedure

2.1. Pilot scale CO_2 capture facility

Elemental partitioning, including emissions tests were carried out in a 25 kWth pilot scale CO_2 capture reactor, comprising a 4.3 m high, 0.1 m diameter, entrained flow bed carbonator, and a 1.2 m high, 0.165 m diameter, bubbling fluidised bed calciner, as shown in Fig. 1. Two cyclones present at the exit of the carbonator, ensure solids recycling to the calciner, and minimise particulate
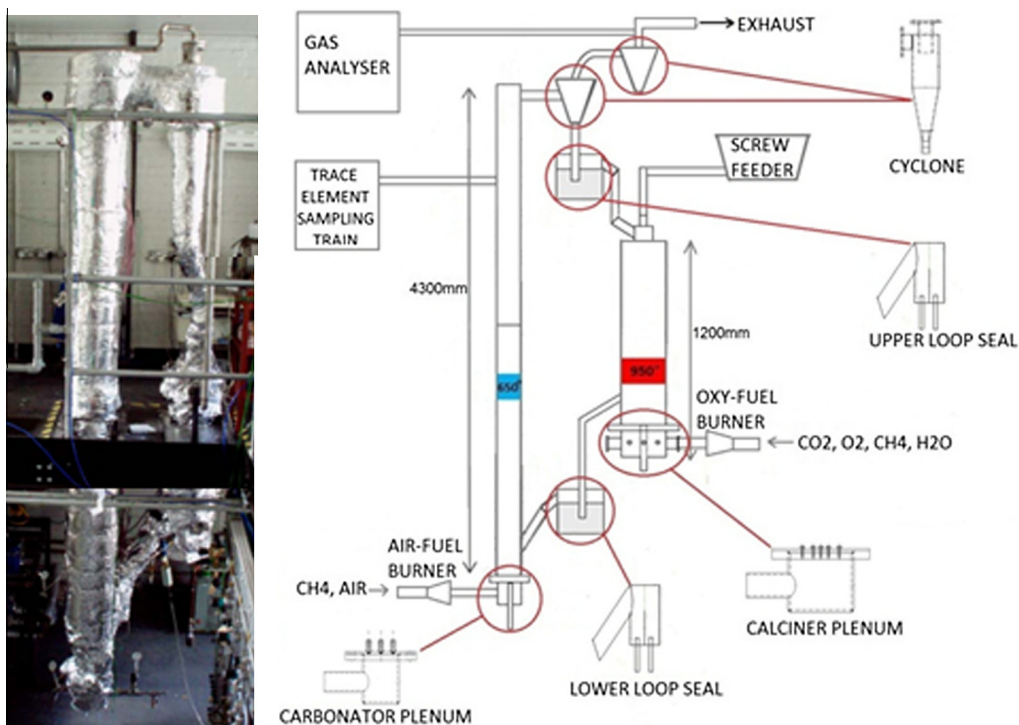
Fig. 1. Diagram of pilot scale 25 kWth CO₂ capture reactor, comprising an air-fired carbonator, and oxy-fired calciner, two cyclones, and an upper and lower loop seal.

emissions to the atmosphere. Two loop seals, one located at the base of the first cyclone leading to the calciner, and the other located between the lower third of the two reactors, allow the controlled transfer of solids between the two reactors, whilst at the same time preventing gas transfer in order to maintain process efficiency. A total of thirteen pressure tappings along the length of the carbonator, and seven pressure tappings along the length of the calciner, allow pressure analysis of the system. Temperatures within the reactors were measured using K-type thermocouples with metal sheaths. Gases were introduced into the reactor using rotameters to ensure accurate flow rates. Continuous looping experiments were undertaken to investigate the effect of 4.5 kg, 6 kg and 13 kg bed inventory, and SO₂ concentrations of 0 ppm, 1000 ppm and 2000 ppm for a bed inventory of 13 kg, on elemental partitioning between solid sorbent and gaseous emissions.

2.2. Sorbent analysis

Inductively Coupled Plasma-Mass Spectrometry (ICP-MS) analysis was undertaken of Longcliffe SP52 limestone from the UK, to determine the quantities of elemental impurities present in the naturally occurring rock, for which the major, minor and trace elements are given in Table 1, and ICP-MS results are provided in Table 2. Throughout the literature, there are varying definitions for major, minor and trace elements. In this case, major elements are defined as those of concentration >10 ppm, minor elements are of concentration between 1 and 10 ppm, and trace elements are of concentration <1 ppm. The ICP-MS process uses high temperature argon plasma to generate positively-charged ions from the sample, allowing concentrations of such ions to then be measured and quantified. Mg appears to be the element found

Table 1
Identification of major, minor, and trace elements in the limestone sorbent used in the CO₂ capture reactor.

Major > 10 ppm	Li, Na, Mg, Al, P, K, Ti, Cr, Mn, Fe, Zn, Ga, Br, Sr, Y, Ba, Pb
Minor (1–10 ppm)	V, Co, Ni, Cu, Zr, Mo, Cd, Sn, La, Ce, Pr, Nd, Sm, Gd, Dy, U
Trace (<1 ppm)	Be, Sc, Ge, As, Se, Rb, Nb, Ru, Pd, Ag, In, Sb, Te, I, Cs, Eu, Tb, Ho, Er, Tm, Yb, Lu, Hf, Ta, W, Re, Os, Pt, Au, Hg, Tl, Th

Table 2
ICP-MS analysis of Longcliffe SP52 limestone identifying the presence of a variety of elements at varying quantities within the limestone sample.

Element (µg/g)	Element (µg/g)	Element (µg/g)	Element (µg/g)	Element (µg/g)	Element (µg/g)
Li 13.89	Ti 19.81	Zn 10.5	Zr 1.41	Ba 135.76	Tb 0.21
Na 136.80	V 9.03	Ga 10.40	Mo 1.45	La 6.78	Dy 1.32
Mg 5749.22	Cr 16.83	Ge 0.35	Ag 0.14	Ce 8.03	Ho 0.31
Al 414.5	Mn 268.35	Se 0.8	Cd 1.5	Pr 1.46	Er 0.90
P 83.60	Fe 354.85	Br 11.99	Sn 2.62	Nd 5.66	Tm 0.13
K 224.51	Co 0.68	Rb 0.87	Sb 0.11	Sm 1.21	Yb 0.60
Ca over-range	Ni 2.98	Sr 763.2	I 0.55	Eu 0.33	Pb 26.21
Sc 0.58	Cu 6.22	Y 16.07	Cs 0.18	Gd 1.41	U 1.31

in the highest concentration (5.75 ppm), as expected given the presence of a dolomitic fraction ($CaMg(CO_3)_2$) in most naturally occurring limestone. Other elements found at higher concentrations appear to be Na, Al, P, K, Mn, Fe, Sr, Ba and Pb, all found at concentrations of over 26 ppb. ICP-MS analysis confirmed the presence of Al and Fe in similar quantities (414.5 and 354.8 ppm respectively). Samples taken after testing were also analysed using ICP-MS and compared to a blank acid digestion sample, to identify changes in elemental concentration as a result of use in the calcium looping cycle process. Ca-derived sorbents sampled before, during and after tests were analysed for changes in morphology using environmental scanning electron microscopy (SEM) and electron dispersive spectroscopy (EDS). The SEM–EDS analysis provides useful data, but due to it having a smaller range than ICP-MS, cannot show data for elements below a certain concentration, and therefore shows data for fewer elements than ICP-MS. Nonetheless, EDS data is useful in outlining trends for the elements which are analysed, and for supporting results achieved using ICP-MS.

2.3. Flue gas analysis

An ADC 7000 gas analyser was used to measure real time on-line levels of CO_2 and O_2 in combustion gases from the carbonator and calciner, during pilot scale CO_2 capture tests. CO_2 and O_2 concentrations from the carbonator for a typical test are provided in Fig. 2.

Elemental sampling from the reactor took place from the carbonator. Although the carbonator operates at lower temperatures (600–700 °C) than the calciner (800–950 °C) and therefore elemental release may be slightly lower due to lower volatility, it was considered that compared to the calciner, the carbonator will be exposed to the flue gas in its entirety, and also in terms of location of the sampling equipment the carbonator was the most suitable reactor from which to sample.

The elemental sampling method was undertaken in accordance with US Environmental Protection Agency (EPA) Method 29: Determination of Metals Emissions from Stationary Sources [23]. The experimental set up, as outlined in Fig. 3, comprises a 'sampling train' consisting of several bubblers through which a stack sample of the flue gas is passed. Several bubblers contain aqueous acidic dilution to allow collection of condensed trace elements in the flue gas which passes through. A pump allows the gas to be sampled through the bubblers, and a dry gas meter allows the recording of the volume of gas which is sampled. A glass filter prevents particulate matter from passing through the bubblers. Prior to, and between each experiment, the glassware is
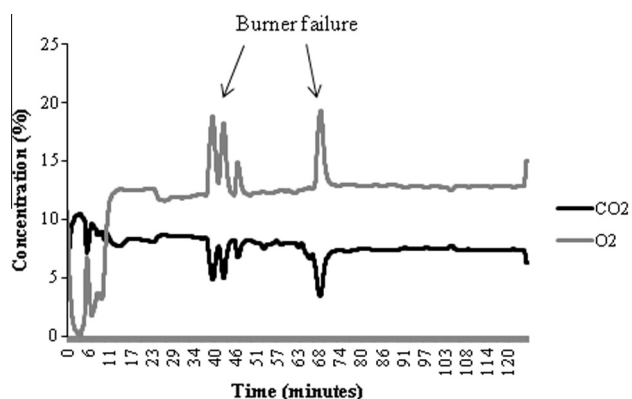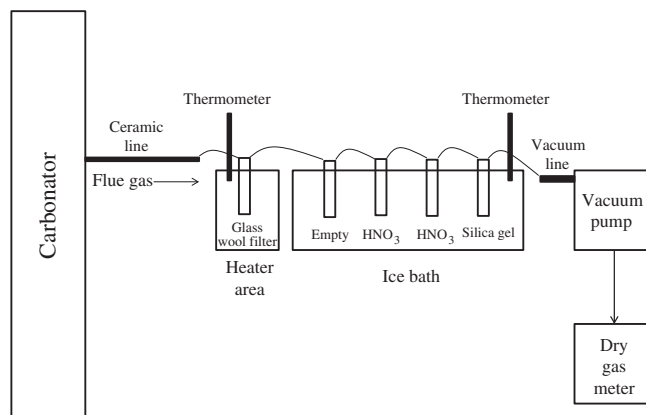

Fig. 3. Trace element emissions sampling train, comprising heated glass filter, bubblers, vacuum pump, and dry gas meter, adapted from EPA Method 29.

acid washed in 10% HNO_3 acid in order to prevent contamination. Further details of the procedure are provided in EPA Method 29 [23].

The sampling system was started as the reactor was heating up, at approximately 30 min prior to the beginning of the experiment. This allowed the sampling of gases for a longer time period, and to take into account any emissions prior to the start of the actual experiment, which may occur as both the reactor material and Ca-based CO_2 sorbent were heated. Although the majority of element release is likely to occur at the start of each test, with emissions likely to decrease to a steady level as looping cycles continue, the sampling of the initial release is important to identify total emissions. Sampling was stopped when the burner was turned off, and therefore at the end of experiment. Results are therefore shown for average test durations of approximately 2 h. Elemental analysis of the acidic solution was carried out using ICP-MS.

2.4. Thermodynamic modelling

Chemical equilibrium models have proven useful in estimating flue gas compositions and elemental partitioning from energy processes [1]. The MTDATA software computes chemical equilibrium based on Gibbs free energy minimisation, allowing the identification of the most prevalent species in a reaction, under specific conditions, including temperature and pressure.

Thermodynamic modelling using MTDATA software was undertaken in addition to pilot scale tests, in a bid to improve understanding of the likely compounds and associated phase formation of elements under carbonation and calcination conditions. Modelling was undertaken for 4 major elements (C, Ca, O, and H) and up to 9 minor elements (Ba, Cd, Cr, K, Mg, Ni, Sr, Ti, and Zn) based on those which are considered to be most volatile, have the greatest negative impact on the environment and health, and which were present in the highest quantities in the limestone as identified by ICP-MS analysis as outlined in Table 2, in order to investigate partitioning behaviour under pilot scale CO_2 capture conditions. The multiphase module of MTDATA was used in the modelling, combined with the Scientific Group Thermodata Europe (SGTE) database, in order to predict compound/phase formation for the complete temperature range, from temperatures of 600 °C, up to 750 °C for carbonation and 1000 °C for calcination, in steps of 20 °C, and at atmospheric pressure. Molar quantities, based on ICP-MS analysis of the limestone, for each of the elements being investigated were entered into the model.

Fig. 2. CO_2 and O_2 concentrations during steady state conditions for a typical test.

3. Results and discussion

3.1. Elemental partitioning – experimental effect of sorbent mass

3.1.1. Major elements

Fig. 4 shows the effect of bed inventory on major element concentration for solid samples taken from the carbonator. Samples were acid digested and analysed using ICP-MS, and compared with acid digestion blanks in order to obtain the final values. The effect of bed inventory is apparent, with concentrations of Fe in particular increasing from 319 ppm to 4598 ppm for bed inventories of 4.5 kg and 13 kg respectively. Similarly, concentrations of Cr, Mn, Zn and Pb also increased with increasing inventory. For Cr, no positive recording was made for the lowest bed inventory of 4.5 kg, but recordings were made at 6 kg and 13 kg. For Mg, Al, Si, Ti, Sr and Y concentrations appeared to slightly decrease with increasing bed inventory.

Results of ICP-MS flue gas analysis provided in Fig. 5 show that most of the major elements present in the carbonator flue gas increase with the mass of the limestone in the reactor. However, some elements are only present for the largest bed inventory of 13 kg e.g., Ti, Cr, and Mn. However, all elements included within Fig. 5 can be considered to be at very low concentrations of <2 ppm.

Those elements at the higher concentrations in the flue gas include Na, Si, K, Zn, and Br. For Na in particular which was present in reduced amounts in the solid, this suggests that some of it may be partitioning to the flue gas for bed inventories 6 and 13 kg.

For Na, Al, K and Fe, the lowest bed inventory of 4.5 kg resulted in a concentration in the flue gas which was less than that of the blank sample, values which then increased for the higher bed

inventories. This suggests that a certain amount of these elements is being absorbed, perhaps by the sorbent in the case of Fe, or by the reactor itself. In the case of P, decreased values compared to the blank were found for bed inventories of 4.5 kg and 13 kg, but an increased value for 6 kg inventory. However, the values are very low at <0.01 ppm and this anomalous result may be due to analytical errors. Overall, although concentrations in the flue gas are small at <2 ppm, increasing bed inventory does appear to increase the concentration of the majority of major elements present in the flue gas.

3.1.2. Minor elements

Fig. 6 shows the concentrations of minor elements in the solid sorbent, where increasing bed inventory resulted in increasing values observed for Co, Ni, Cu, Mo, Cd, and Sn. In the case of Cu and Sn, values were obtained that were lower than that of the blank for a bed inventory of 4.5 kg, which then increased to values of 22 and 0.22 ppm respectively for 13 kg. In the case of Gd, Dy and U, small decreases in concentration were found for an increasing inventory, however values are low at <1 ppm and the changes observed are small. The remaining elements (Zr, Le, Ce, Pt, and Nd) recorded an increase in concentration for 6 kg over 4.5 kg, and then a decrease from 6 kg to 13 kg. All minor element flue gas concentrations were <0.1 ppm and therefore considered negligible.

3.1.3. Trace elements

Fig. 7 shows solid concentrations of trace elements, of which only Rb, Nb and W were found at concentrations greater than 0.1 ppm. W showed the greatest change, with concentration increasing from 0.06 to 0.42 to 0.74 ppm for inventories 4.5, 6 and 13 kg respectively. All trace element flue gas concentrations
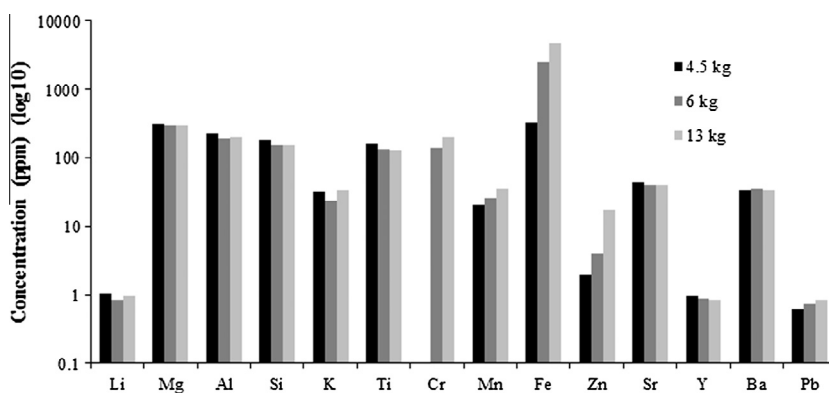

Fig. 4. Effect of bed inventory on increase of solid major elemental concentrations for bed inventories of 4.5 kg, 6 kg and 13 kg CaCO$_3$.
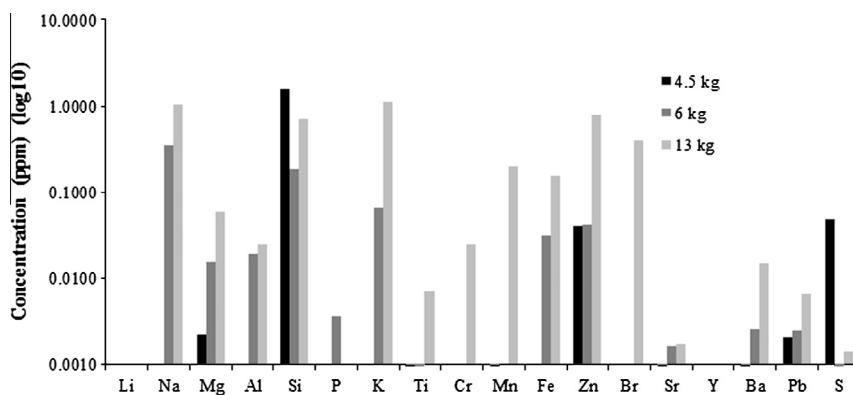

Fig. 5. Effect of bed inventory on increase of flue gas major elemental concentrations for bed inventories of 4.5 kg, 6 kg and 13 kg CaCO$_3$.
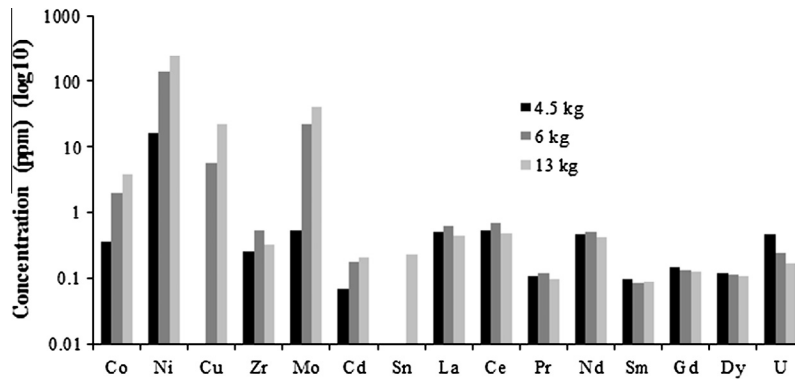
Fig. 6. Effect of bed inventory on increase of solid minor element concentrations for bed inventories of 4.5 kg, 6 kg and 13 kg $CaCO_3$.
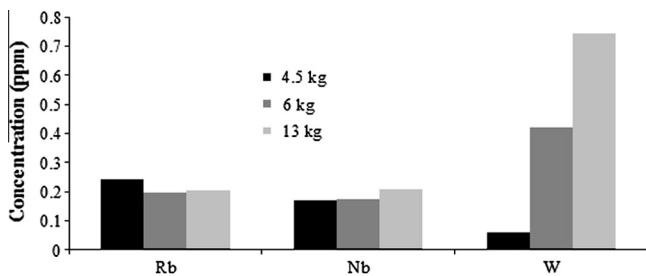

Fig. 7. Effect of bed inventory on increase of solid trace elemental concentrations, for bed inventories of 4.5 kg, 6 kg and 13 kg $CaCO_3$.

were found at a concentration of <0.1 ppm and therefore considered negligible.

As expected for major, minor and trace elements, the concentration is generally higher by several orders of magnitude for solids samples compared to flue gas samples. It is clear that in the cases where elemental concentration decreased with increasing bed inventory, this is mostly seen for period 3 elements (Mg, Al, and Si), and some lanthanide rare earth metals (Sm, Gd, Dy, and Rb) and U.

The geochemistry of limestone is complex, with various hydrous and anhydrous forms of the mineral available. Naturally formed $CaCO_3$ (termed '$CaCO_3$ I' for the purposes of this study) generally has a rhombohedral-hexagonal lattice system, and is stable at atmospheric pressures and Longcliffe SP52 can be assumed to be in this form. Other forms of $CaCO_3$ (II-V) are formed over ranges of both increasing temperature and pressure [24].

Each Ca^{2+} in the $CaCO_3$ structure is bonded with six oxygen atoms, resulting in a charge of +1/3 per bond. Similarly, the O in each CO_3 group is bonded with two Ca^{2+} ions, meaning each CO_3 group is coordinated to six Ca ion. This provides alternating layers of Ca and CO_3 groups [25].

Elemental impurities have three possible locations for bonding in $CaCO_3$ [26]:

- Substitution via cation exchange for Ca^{2+} occurs for 90–95% of elements e.g., Fe, Mn, and Sr.
- Adsorption onto crystal faces to balance charge inbalances e.g., Na, and K.
- Inclusion of additional mineral phases within the $CaCO_3$.

Due to the hexagonal structure of the crystals, spaces between the cations allow elements with an ionic radii smaller than Ca^{2+}, such as Fe, Mn, Cd, Co, Ni, Zn, and Cu to be incorporated with the crystal structure.

For the cases where elemental concentration increased with increasing bed inventory, the elements concerned were mostly those of low volatility (Be, Cr, and Mn), transition metals (Fe, Co, Ni, Cu, Zn, Nb, Mo, Rh, Cd, and W), and group 6 metals (Pb, and Sn). Elements that have low volatility are most likely to partition to solid phases within the reactor, and therefore it would be expected that the concentration of the low volatility elements would increase for a greater bed inventory. The transition metals have high melting points because of strong metallic bonds resulting from the presence of unpaired electrons, resulting in low volatility. Most also have a charge of 2+, allowing substitution for Ca^{2+} within the $CaCO_3$ lattice. Iron oxides are also able to sequester transition metal cations and thus are able to immobilise other transition metal impurities [27], thus accounting for the general increase in transition metal concentration with bed inventory.

For Pb and Sn, of which Pb is considered to be a Group II element, and Sn is considered to be between Group I and Group II, both are emitted mostly in coal fly ashes in coal combustion [28], and therefore could be considered to partition to the solid phase in the calcium looping cycle.

Further, it was noted that non-volatile elements have been found more likely to condense out with particulate matter, resulting in an increase in trace element concentration with a decrease in sorbent size [3,29]. Sager [8] found that introduction of limestone increased Pb, Cd and Mn emissions, but these were immediately sorbed from the vapour phase onto particulates.

With regards to the elemental species that decrease in concentration with increasing bed inventory, Mg, Al and Si oxides are generally considered primary components of limestone in addition to Ca. However, no Si was detected from ICP-MS analysis of unreacted limestone, which can be attributed to low Si detection limits on the ICP-MS in question; although EDS analysis shows decreasing Si concentrations with increasing bed inventory (Fig. 8). MgO and Al_2O_3 can be considered to have extended ionic structures, whilst
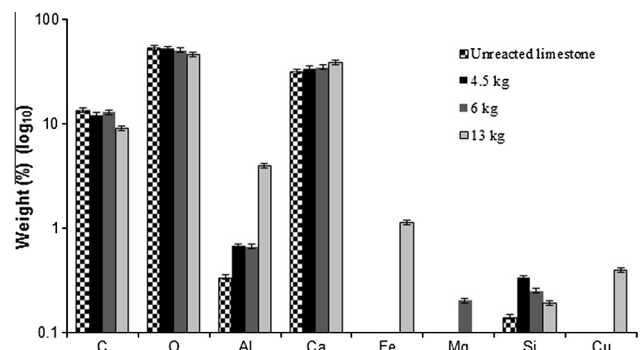

Fig. 8. SEM–EDS analysis of sorbent for reactions undertaken with different sorbent masses, showing error bars of +1%.

Table 3

Mass balance for major, minor and trace elements showing the effect of 4.5 kg, 6 kg and 13 kg bed inventory.

		Units	Major elements																
			Li	Na	Mg	Al	Si	P	K	Ti	Cr	Mn	Fe	Zn	Br	Sr	Y	Ba	Pb	S
4.5 kg	Solid samples in	µg/min	1275.699	−146458	380561.4	271745.8	220610.8	−3397.42	38136.24	190323.7	0	25249.51	383901.2	2344.059	−2236.7	53738.15	1143.107	39787.82	728.1889	−74437.1
	Gaseous samples out	µg/min	−1.1E−05	−0.0406	0.000781	−0.01538	0.547387	−0.00255	−0.00809	0.000153	−0.00022	5.21E−05	−0.00153	0.013862	−0.00057	0.000252	−1E−06	0.000181	0.000728	0.016624
	Mass balance closure (out/in)	n/a	**−9E−09**	**2.77E−07**	**2.05E−09**	**−5.7E−08**	**2.48E−06**	**7.5E−07**	**−2.1E−07**	**8.04E−10**	**0**	**2.06E−09**	**−4E−09**	**5.91E−06**	**2.55E−07**	**4.69E−09**	**−9.1E−10**	**4.54E−09**	**1E−06**	**−2.2E−07**
6 kg	Solid samples in	µg/min	1006.732	−146268	362501.7	225106.8	181554.6	−3410.96	28652.52	160520.8	170327.7	31202.58	3026590	4816.438	−2206.5	48049.55	1050.646	42856.2	887.4364	−73432
	Gaseous samples out	µg/min	−2E−05	0.119243	0.005338	0.00655	0.064094	0.001281	0.022625	0.000123	−0.00029	−0.0002	0.010926	0.014225	−1.5E−05	0.00056	−1.2E−05	0.000877	0.000863	0.000188
	Mass balance closure (out/in)	n/a	**−2E−08**	**−8.2E−07**	**1.47E−08**	**2.91E−08**	**3.53E−07**	**−3.8E−07**	**7.9E−07**	**7.67E−10**	**−1.7E−09**	**−6.3E−09**	**3.61E−09**	**2.95E−06**	**6.61E−09**	**1.17E−08**	**−1.2E−08**	**2.05E−08**	**9.72E−07**	**−2.6E−09**
13 kg	Solid samples in	µg/min	1146.613	−136231	350820.9	238635.9	180748.1	−1919.96	40808.64	150490.5	243975.7	41403.88	5514952	20423.48	−2081.45	48024.37	1012.59	40272.33	1004.837	−69270.4
	Gaseous samples out	µg/min	−0.00012	0.35837	0.020767	0.008507	0.241046	−0.0036	0.382791	0.002462	0.008477	0.067894	0.053066	0.271775	0.139514	0.000604	−1E−05	0.005187	0.002288	0.000491
	Mass balance closure (out/in)	n/a	**0**	**−2.6E−06**	**5.92E−08**	**3.56E−08**	**1.33E−06**	**1.88E−06**	**9.38E−06**	**1.64E−08**	**3.47E−08**	**1.64E−06**	**9.62E−09**	**1.33E−05**	**−6.7E−05**	**1.26E−08**	**−9.9E−09**	**1.29E−07**	**2.28E−06**	**−7.1E−09**

		Units	Minor elements													
			V	Co	Ni	Cu	Zr	Mo	Cd	Sn	La	Ce	Pr	Nd	Gd	Dy	U
4.5 kg	Solid samples in	µg/min	0	435.3898	19692.76	−803.412	297.7981	644.396	82.84071	−124.975	619.4009	634.1599	128.3079	543.9397	170.9185	141.6386	537.2744
	Gaseous samples out	µg/min	0	−0.00022	−0.00415	0.001208	−0.00093	0	4.27E−05	0.00172	−3.5E−07	−1E−05	−6.9E−07	−2.1E−06	0	0	−1E−06
	Mass balance closure (out/in)	n/a	**0**	**−5.1E−07**	**−2.1E−07**	**−1.5E−06**	**−3.1E−06**	**0**	**5.15E−07**	**−1.4E−05**	**−5.6E−10**	**−1.6E−08**	**−5.4E−09**	**−3.8E−09**	**0**	**0**	**−1.9E−09**
6 kg	Solid samples in	µg/min	0	2423.014	173928.6	6961.409	648.8454	26191.47	207.593	−123.288	738.317	828.2583	141.3699	607.7495	158.7476	132.681	282.5049
	Gaseous samples out	µg/min	−1E−05	−0.00029	−0.01179	0.001385	−0.00173	−6.9E−07	3.26E−05	0.000758	−1.4E−06	−8.5E−05	−5.2E−06	−1.7E−05	0	0	−2.4E−06
	Mass balance closure (out/in)	n/a	**0**	**−1.2E−07**	**−6.8E−08**	**1.99E−07**	**−2.7E−06**	**−2.6E−11**	**1.57E−07**	**−6.1E−06**	**−1.9E−09**	**−1E−07**	**−3.7E−08**	**−2.8E−08**	**0**	**0**	**−8.6E−09**

Table 3 (*continued*)

	Units	Major elements																	
		Li	Na	Mg	Al	Si	P	K	Ti	Cr	Mn	Fe	Zn	Br	Sr	Y	Ba	Pb	S
13 kg Solid samples in	µg/min	0	4460.402	302682.4	26986.38	385.2317	48063.8	244.7849	272.0325	533.4318	572.8632	117.4082	494.2219	145.5418	125.8261	197.6001			
Gaseous samples out	µg/min	0.000995	0.008477	0.015103	0.039212	0.000118	1.18E−05	0.000174	0.003293	−4.5E−06	−0.00016	−2E−05	−8.9E−05	0	0	0			
Mass balance closure (out/in)	n/a	**0**	**1.9E−06**	**4.99E−08**	**1.45E−06**	**3.06E−07**	**2.45E−10**	**7.12E−07**	**1.21E−05**	**−8.5E−09**	**−2.9E−07**	**−1.7E−07**	**−1.8E−07**	**0**	**0**	**0**			

|	Units	Trace elements		
		Rb	Nb	W
4.5 kg Solid samples in	µg/min	291.8469	204.9593	71.17635
Gaseous samples out	µg/min	−8.7E−06	3.47E−07	4.51E−06
Mass balance closure (out/in)	n/a	**−3E−08**	**1.69E−09**	**6.34E−08**
6 kg Solid samples in	µg/min	237.6517	210.411	506.5362
Gaseous samples out	µg/min	−1.8E−05	−2.1E−06	3.82E−06
Mass balance closure (out/in)	n/a	**−7.6E−08**	**−9.9E−09**	**7.54E−09**
13 kg Solid samples in	µg/min	244.1204	249.6585	892.9666
Gaseous samples out	µg/min	3.61E−05	0	−0.00023
Mass balance closure (out/in)	n/a	**1.48E−07**	**0**	**−2.6E−07**

The bold values meant to be final outcomes
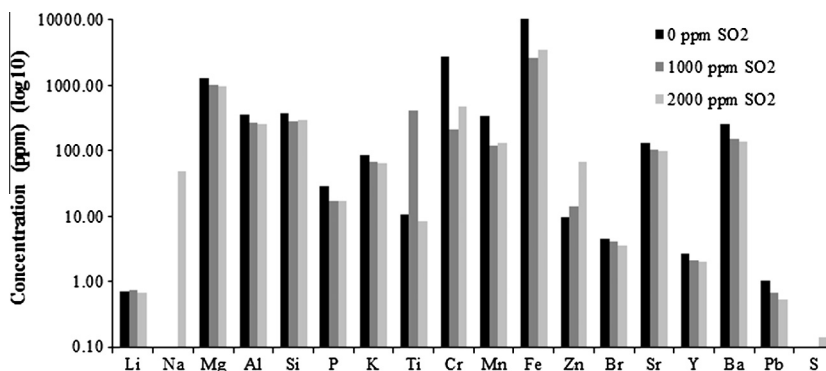
Fig. 9. Effect of SO_2 on (a) increase of solid major elemental concentrations for SO_2 concentrations of 0 ppm, 1000 ppm and 2000 ppm, and bed inventory of 13 kg $CaCO_3$.
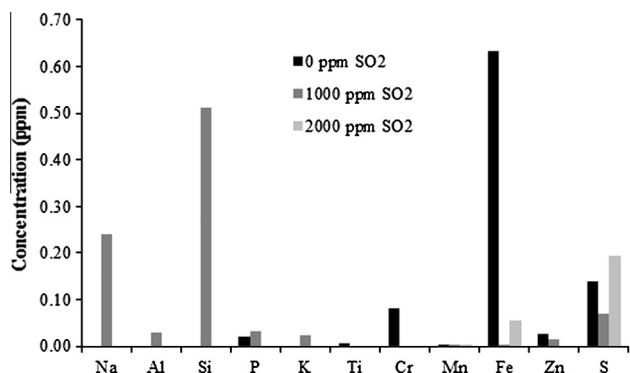

Fig. 10. Effect of SO_2 on increase of flue gas major elemental concentrations for SO_2 concentrations of 0 ppm, 1000 ppm and 2000 ppm, and bed inventory of 13 kg $CaCO_3$.

SiO_2 has an extended covalent structure, meaning that all have high melting and boiling points, requiring large amounts of energy to volatilize them. Therefore, they are considered to be of low volatility, but the increase of these elements in the flue gas analysis suggests that they are being removed from the sorbent under the high temperature conditions in the fluidised bed.

The literature suggests that limestone can be used to capture Ni, Pb and Cd, thus accounting for the increased concentration of these three elements with increasing bed inventory [30]. By contrast, it has also been suggested that interaction, and therefore capture of Ni with Ca-bearing materials is of minor significance [31] although it would appear that this is not the case in this study.

With regard to the lanthanides, when investigating limestone formation and rare earth element prevalence, Nagarajan et.al.

[32] found a negative correlation of rare earth elements and CaO. It is suggested that in general the absorption of lanthanide cations is weak, and therefore they have low molar absorption coefficients, due to shielding of the $4f$ orbitals by the filled $5s$ and $5p$ sub-shells [33]. The low cation exchange capacity of the lanthanides may explain the small decreases in concentration in limestone, with increasing bed inventory.

3.1.4. Mass balance

A mass balance for the carbonator is provided as Table 3 calculated based on the incoming and outgoing concentrations of elements. It shows that partitioning was always higher to the solid samples than in the flue gas samples, with very low concentrations portioning to the flue gas in all cases.

3.1.5. SEM–EDS analysis

SEM–EDS analysis of sorbent sampled from the carbonator after each test was undertaken to determine the percentage weight of the elemental species present. The results as shown in Fig. 8 confirm that increasing bed inventory generally increases the presence of Al, Fe and Cu. Al was identified in the unreacted sample at a weight% of 0.34, but this increased to similar values of 0.67% and 0.66% for 4.5 kg and 6 kg samples respectively, with a much higher value of 3.98% for 13 kg sample of sorbent. This increase in Al% weight with increasing sorbent mass may be because there is a greater amount of Al present originally, or because the limestone acts as a sorbent for Al, which is also considered the case for Fe and Cu. Further, Al is likely to form Ca aluminates which are important constituents of cement. The EDS results indicate similar quantities of C, O and Ca between tests, although values for the samples that had undergone testing are slightly lower for C and O, and slightly higher for Ca, compared to the unreacted limestone sample, implying that the small change was a result of chemical
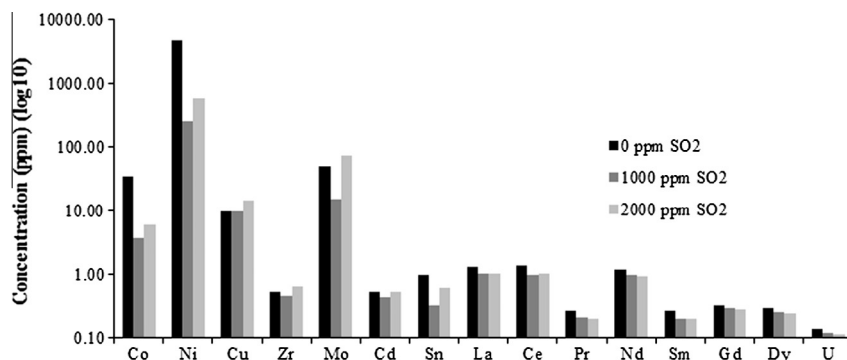

Fig. 11. Effect of SO_2 on (a) increase of solids minor elemental concentrations for SO_2 concentrations of 0 ppm, 1000 ppm and 2000 ppm, and bed inventory of 13 kg $CaCO_3$.

reactions. Although the values are small, a steady decrease in Si weight% was recorded with increasing sorbent mass, implying removal of Si from limestone in the capture process. However the lowest value was recorded for the unreacted limestone.

3.2. Elemental partitioning – experimental effect of SO$_2$ concentration

3.2.1. Major elements

Fig. 9 shows that increasing SO$_2$ concentration has some effect on major element concentration in solids. Concentrations of Mg, Al, Si, P, K, Br, Sr, Y, Ba and Pb appear to decrease as SO$_2$ concentration increases. However, there appears to be little difference between concentrations for 1000 and 2000 ppm, the greatest change in concentration being from 0 to 1000 ppm SO$_2$. The trend in the batch experiments whereby concentrations of elements at 1000 ppm were generally lower than at 0 and 2000 ppm, is also seen for some elements in the looping cycle test including Cr, Mn and Fe, but not to the same extent as was seen in the batch tests. Ti shows the same trend for these tests as for single column tests, with 1000 ppm SO$_2$ showing higher concentrations of Ti (135 ppm for single column, 407 ppm for looping test) compared to 0 and 2000 ppm SO$_2$ at values close to 10 ppm Ti in both tests. Zn is the only major element showing a clear increase in concentration with SO$_2$, increasing from 9.4 to 14.1 to 66.8 ppm for SO$_2$ concentrations of 0, 1000 and 2000 ppm respectively.

Fig. 10 shows how gaseous major element concentrations were affected by flue gas SO$_2$ concentration. Concentrations of all were very low at <1 ppm, with Fe and Si present in the highest concentrations at 0.63 and 0.51 ppm respectively. For several elements, 1000 ppm SO$_2$ resulted in either the highest concentrations, as was the case for Na, Al, and Si, or the lowest concentrations, as was the case for Fe, when compared to 0 and 2000 ppm SO$_2$.

3.2.2. Minor elements

1000 ppm SO$_2$ concentration in looping cycle tests again appears to have some influence in reducing the concentration of some minor elements in the sorbent, when compared to 0 and 2000 ppm SO$_2$ (Fig. 11). This is the case for the elements Co, Ni, Zr, Mo, Cd, Sn and Ce. For the remainder of the elements shown, there was a small decrease in value with increasing SO$_2$, other than for Cu which saw a small increase in value from 9.74 to 14.13 ppm for 0 ppm and 2000 ppm SO$_2$ respectively. All minor element flue gas concentrations were <0.1 ppm and therefore considered negligible.

3.2.3. Trace elements

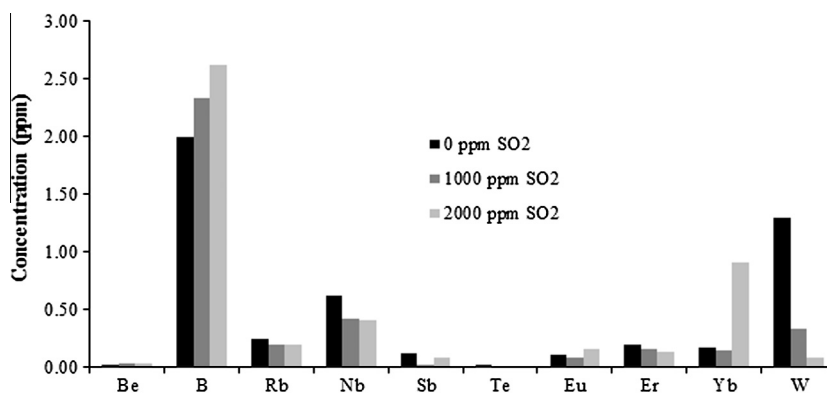Fig. 12 shows that increasing SO$_2$ concentration does influence trace element sorbent concentration, and for B in particular, concentrations rose from 2 ppm to 2.6 ppm for 0 and 1000 ppm SO$_2$ respectively. W showed a decrease with increasing SO$_2$ concentration from 1.3 ppm to 0.08 ppm for 0 and 1000 ppm SO$_2$ respectively. Although trends are evident for the trace elements, concentrations are low, reducing the reliability of the results and in turn affecting the reliability of the trends observed. All trace element flue gas concentrations were <0.1 ppm and therefore considered negligible.

The results show that looping cycle tests carried out in the presence of increasing concentrations of SO$_2$ resulted in, for the most part, a decrease in elemental concentrations in both solid sorbent and flue gas samples. A small number of elements appeared to increase in concentration with increasing SO$_2$ concentration, including Zn, Cu, B and Yb. Iron cation exchange sites may account for the increase in concentration of the transition metals Zn and Cu. The larger molar volume of CaSO$_4$ (46 cm^3/mol) compared to CaCO$_3$ (37 cm^3/mol) may affect ion-exchange or covalent bonding within the pore structure, causing enhanced trace element release in the majority of cases. The fact that emissions do not increase linearly with increasing sorbent mass or SO$_2$ concentration implies that the chemistry of the system is complex.

3.2.4. Mass balance

A mass balance showing effects of increasing SO$_2$ concentration on elemental partitioning for the carbonator is provided as Table 4, calculated based on the incoming and outgoing concentrations of elements. A mass balance closure value of 1 indicates outgoing concentrations equal to incoming concentrations, and as shown by the low closure values, partitioning was always higher to the solid samples than in the flue gas samples, with very low concentrations portioning to the flue gas.

3.2.5. SEM–EDS analysis

Fig. 13 confirms that SO$_2$ concentration appears to have had an effect on C, O and Ca weight%, with C and O decreasing with increasing SO$_2$, and Ca increasing slightly with increasing SO$_2$. This suggests that the presence of SO$_2$ decreases the extent to which CaO is able to convert to carbonate in the carbonator, the reactor from which the solid samples were taken. It is widely accepted that the presence of SO$_2$ during the carbonation reaction produces CaSO$_4$ on the sorbent particle pore surfaces, which reduces the extent to which CO$_2$ can diffuse into pore space and react to form CaCO$_3$ [34]. As expected, the weight% of S present in the sorbent samples increased from 0.81% to 4.73%, to 10.32% for SO$_2$ concentrations of 0, 1000 and 2000 ppm respectively, with a value of 0% for unreacted limestone. The value of 0% for unreacted limestone, but the presence of S identified during ICP-MS analysis (Table 2) may be due to the higher range that ICP-MS analysis can undertake. In terms of other element species, an SO$_2$ concentration of

Fig. 12. Effect of SO$_2$ on increase of solids trace elemental concentrations for SO$_2$ concentrations of 0 ppm, 1000 ppm and 2000 ppm, and bed inventory of 13 kg CaCO$_3$.

Table 4
Mass balance for major, minor and trace elements showing the effect of 0 ppm, 1000 ppm and 2000 ppm SO$_2$.

Major elements	Units	C	Li	Na	Mg	Al	Si	P	K	Ti	Cr	Mn	Fe	Zn	Br	Sr	Y	Ba	Pb	S	Ga
0 ppm																					
Solid samples in	µg/min	−294050	868.1511	−32777.2	1526918	426314.2	449530.5	34032.52	101167.9	12874.59	3284404	413667.7	21054172	11329.86	5540.994	159610.7	3240	302223	1260.119	−42992.9	600.2396
Gaseous samples out	µg/min	−0.25149	−5.90E−06	−0.50866	−0.00182	−0.02364	−0.02194	0.006793	−0.01158	0.001732	0.028169	0.000131	0.219586	0.009444	−0.00042	−5.20E−06	−9.00E−06	−5.40E−05	−1.63E−03	4.87E−02	6.94E−07
Mass balance closure (out/in)	n/a	**8.55E−07**	**−6.80E−09**	**1.55E−05**	**−1.20E−09**	**−5.50E−08**	**−4.90E−08**	**2.00E−07**	**−1.10E−07**	**1.35E−07**	**8.58E−09**	**3.17E−10**	**1.04E−08**	**8.34E−07**	**−7.50E−08**	**−3.30E−11**	**−2.80E−09**	**−1.80E−10**	**−1.30E−06**	**−1.10E−06**	**1.16E−09**
1000 ppm																					
Solid samples in	µg/min	−148240	886.2451	−14059.9	1229014	316214.9	343609.3	20566.01	80207.19	488837.3	252730	144306.9	3125555	16916.68	4952.253	123817.9	2591.146	180717.2	821.9763	−6529.8	0
Gaseous samples out	µg/min	−0.27001	−0.0006	0.08294	−6.90E−06	0.010574	0.177463	0.011236	0.00778	−0.00082	−9.50E−05	0.000126	0.001092	0.004723	−0.00095	6.07E−05	6.94E−06	0.000477	−0.01281	0.024124	−1.00E−06
Mass balance closure (out/in)	n/a	**1.82E−06**	**−6.80E−07**	**−5.90E−06**	**−5.60E−12**	**3.34E−08**	**5.16E−07**	**5.46E−07**	**9.70E−08**	**−1.70E−09**	**−3.80E−10**	**8.70E−10**	**3.49E−10**	**2.79E−07**	**−1.90E−07**	**4.90E−10**	**2.68E−09**	**2.64E−09**	**−1.60E−05**	**−3.70E−06**	**0.00E+00**
2000 ppm																					
Solid samples in	µg/min	−147286	7.96E+02	58844.77	1.18E+06	309987.9	3.48E+05	20374.41	7.82E+04	10020.1	5.66E+05	155200.5	4.24E+06	80212.22	4.24E+03	1.19E+05	2.45E+03	1.69E+05	6.34E+02	1.73E+02	0.00E+00
Gaseous samples out	µg/min	−0.64789	−2.90E−05	−0.14338	−6.35E−03	−0.02401	−4.79E−02	−0.04158	−1.33E−02	−0.005	−2.70E−04	8.71E−05	1.93E−02	−5.82E−03	−7.10E−04	−2.80E−04	−1.10E−05	−5.00E−04	−2.06E−03	6.73E−02	−5.90E−06
Mass balance closure (out/in)	n/a	**4.40E−06**	**−3.70E−08**	**−2.40E−06**	**−5.40E−09**	**−7.70E−08**	**−1.40E−07**	**−2.00E−06**	**−1.70E−07**	**−5.00E−07**	**−4.80E−10**	**5.61E−10**	**4.55E−09**	**−7.30E−08**	**−1.70E−07**	**−2.30E−09**	**−4.40E−09**	**−3.00E−09**	**−3.30E−06**	**3.89E−04**	**0.00E+00**

Minor elements	Units	V	Co	Ni	Cu	Zr	Mo	Cd	Sn	La	Ce	Pr	Nd	Sm	Gd	Dy	U
0 ppm																	
Solid samples in	µg/min	0	40468.87	5836673	11689.38	625.0497	61476.98	637.9324	1196.899	1556.183	1612.962	323.499	1428.072	328.7475	398.4095	359.2843	165.8052
Gaseous samples out	µg/min	−1.10E−05	8.19E−05	−0.00053	−0.00018	−0.00485	−7.60E−06	1.08E−05	0.002141	0	−4.30E−05	−1.40E−06	−5.90E−06	−6.90E−07	−1.00E−06	−1.00E−06	−1.10E−05
Mass balance closure (out/in)	n/a	**0**	**2.02E−09**	**−9.10E−11**	**−1.60E−08**	**−7.80E−06**	**−1.20E−10**	**1.69E−08**	**1.79E−06**	**0.00E+00**	**−2.60E−08**	**−4.30E−09**	**−4.10E−09**	**−2.10E−09**	**−2.60E−09**	**−2.90E−09**	**−6.50E−08**
1000 ppm																	
Solid samples in	µg/min	0	4569.012	312779.5	11942.85	548.3004	18301.66	510.1186	398.419	1233.913	1163.953	249.4852	1169.644	246.166	356.4427	308.3004	143.2411
Gaseous samples out	µg/min	0	−1.70E−05	−0.00209	0.000596	−0.00015	−5.40E−05	−0.00141	0.003546	−6.60E−05	8.05E−05	2.43E−06	6.94E−06	6.94E−07	2.43E−06	6.94E−07	7.91E−05
Mass balance closure (out/in)	n/a	**0**	**−3.80E−09**	**−6.70E−09**	**4.99E−08**	**−2.70E−07**	**−3.00E−09**	**−2.80E−06**	**8.90E−06**	**−5.30E−08**	**6.92E−08**	**9.74E−09**	**5.93E−09**	**2.82E−09**	**6.81E−09**	**2.25E−09**	**5.52E−07**
2000 ppm																	
Solid samples in	µg/min	0	7.43E+03	685066.4	16951.28	775.7853	8.85E+04	6.30E+02	743.5751	1.25E+03	1.26E+03	2.47E+02	1.13E+03	2.39E+02	3.44E+02	2.97E+02	1.37E+02
Gaseous samples out	µg/min	0	−3.50E−07	−0.00102	−0.00126	−0.00304	1.11E−05	−1.40E−05	0.000943	1.80E−05	−9.80E−05	−3.10E−06	−1.10E−05	−3.10E−06	−1.70E−06	−2.80E−06	−2.70E−05
Mass balance closure (out/in)	n/a	**0**	**−4.70E−11**	**−1.50E−09**	**−7.40E−08**	**−3.90E−06**	**1.25E−10**	**−2.20E−08**	**1.27E−06**	**1.44E−08**	**−7.70E−08**	**−1.30E−08**	**−1.00E−08**	**−1.30E−08**	**−5.00E−09**	**−9.30E−09**	**−2.00E−07**

Trace elements	Units	Rb	Nb	W
0 ppm				
Solid samples in	µg/min	289.6223	747.674	1557.614
Gaseous samples out	µg/min	−1.90E−05	−1.70E−06	−1.40E−06
Mass balance closure (out/in)	n/a	**−6.60E−08**	**−2.30E−09**	**−8.90E−10**
1000 ppm				
Solid samples in	µg/min	236.4427	510.83	403.3992
Gaseous samples out	µg/min	1.01E−05	−6.90E−07	−1.90E−05

Table 4 (continued)

Major elements	Units	C	Li	Na	Mg	Al	Si	P	K	Ti	Cr	Mn	Fe	Zn	Br	Sr	Y	Ba	Pb	S	Ga
Mass balance closure (out/in)	n/a	**4.26E−08**	−1.40E−09	**−4.80E−08**																	
2000 ppm																					
Solid samples in	μg/min	2.31E+02	4.90E+02	1.09E+03																	
Gaseous samples out	μg/min	−1.80E−05	0.00E+00	−3.80E−06																	
Mass balance closure (out/in)	n/a	**−7.70E−08**	0.00E+00	**−3.50E−09**																	

The bold values meant to be final outcomes
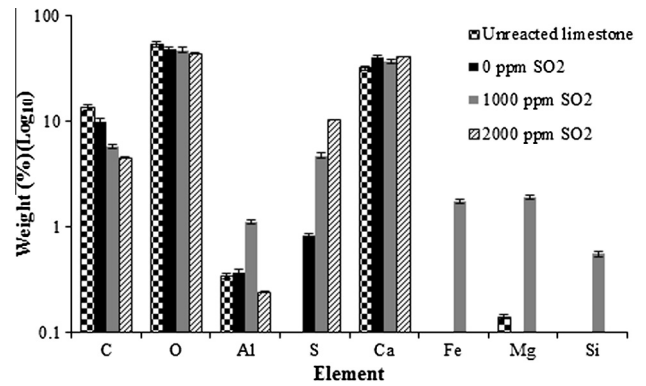
Fig. 13. SEM–EDS analysis of sorbent for reactions undertaken with different SO_2 concentrations, showing error bars of +1%.

1000 ppm appears to result in higher weight% values for Al, Fe, Mg and Si, than for SO_2 concentrations of 0 ppm and 2000 ppm SO_2, with Fe, Mg and Si not present at other SO_2 concentrations. This result is unexpected, but it may be that, as mentioned previously in Section 3.2 the higher concentration of SO_2, and in turn $CaSO_4$, results in greatly reduced available pore space and therefore bonding between these species, when compared to 1000 ppm SO_2. In turn, it may be that the presence of 1000 ppm SO_2 causes some corrosion of the stainless steel reactor itself, resulting in small deposits on the sorbent particles, although it would be expected that if this were the case, higher values would also be achieved for 2000 ppm SO_2. Miller et al. [35] investigated the influence of SO_2 on trace element behaviour during wood-bark combustion, and concluded that SO_2 increased emissions of Cd, but reduced emissions of As and Hg. Overall, it is apparent that the interactions that take place in the presence of SO_2 are complex.

3.3. Thermodynamic modelling – sensitivity analysis

A sensitivity analysis was carried out using MTDATA, in order to determine the effect of the presence of certain trace elements on the formation of compounds. The analysis was carried out using the statistical method 'non-parametric Kruskal–Wallis ANOVA by ranks', using STATISTICA software (CSS Statistica/W, Release 5.0 with Industrial units, Statsoft UK). This method allows the comparison of two or more independent samples, and uses the sum of the difference between mean ranks of the samples, as the statistic. This then provides an indication of whether the absence of an element input to the model has an effect on the stability of a certain compound in the model output.

Due to extended calculation times required, a sensitivity analysis was carried out firstly for nine trace elements (Ba, Cd, Cr, K, Mg, Ni, Sr, Ti, and Zn) and then for twenty-one trace elements (Li, Be, Mg, Al, K, Ti, V, Cr, Mn, Fe, Co, Ni, Zn, As, Se, Sr, Cd, Sb, Ba, Hg, and Pb), in addition to the four 'base' elements (Ca, C, O, and H) (always considered to be present from limestone and gas input), based on those which are considered to be most volatile, have the greatest negative impact on the environment and health, and which were present in the highest quantities in the limestone as identified by ICP-MS analysis, as outlined in Table 2. MTDATA was run for all of 'base' elements and either the nine or twenty-one trace elements present, and the data recorded. One trace element was then removed to see the effect on compound stability and formation. For the next run, this trace element was included, and the next trace element removed, and so on.

The results for carbonation and calcination respectively, are shown in Tables 5 and 6. The results identify that for both carbonation and calcination, Mg has a strong link with the presence of many compounds, including $CaCO_3$. In the case of the sensitivity

analysis based on 9 elements, Mg appears to be the only element that has a link with the presence of compound formation in the model output. However, in the case of the sensitivity analysis based on 21 elements, a greater number of elements have an link with the presence of compounds formed under carbonation conditions, including Mg and Al, having an effect on the greatest number of compounds.

The increased number of elements that have an effect on the presence of compounds under calcination conditions compared to carbonation conditions again may be due to the increased temperatures at which calcination is carried out, thus allowing the less volatile elements to react, due to an increased amount of thermal energy available for activation energies. It is also apparent that increasing the number of trace elements present in the model, increases the chemical interactions that are likely to take place. For example, when 21 trace elements are included in the model in addition to the four base elements, there are a greater number of compounds that are affected by the presence or absence of another trace element, compared to when only 9 elements are included in the model.

3.4. Thermodynamic modelling – effect of sorbent mass

MTDATA estimates of the likely compound formation and associated phases for varying quantities of sorbent, are shown in Figs. 14–16. The results identify that under carbonation conditions the molar quantities of species in equilibrium with combustion gases and limestone, increase as sorbent mass in the reactor increases, and results appear consistent with experimental data for transition metals in particular (Figs. 4–6). Values for gaseous Cd concentrations increased from 8.0E−05 for 4.5 kg, to 6.0E−05 for 6 kg, to 2.0E−04 for 13 kg, at 740 °C. Similarly for Zn, molar gaseous emissions increased from 9.0E−04 for 4.5 kg, to 7.0E−4 for 6 kg, to 2.0E−03 for 13 kg, at all temperatures. These trends are consistent with the majority of the species present. Gaseous KOH concentrations however reaches its maximum value at 720 °C for 4.5 kg, before then declining in value, whereas for 6 kg and 13 kg, the temperature at which the maximum value is reached at 740 °C and 760 °C respectively. This shows the effect that increasing mass has on the thermodynamic equilibrium for a minority of species present.

Table 5
MTDATA sensitivity analysis results for 9 elements.

		Compound presence significantly affected by absence of trace element in model		
		CaCO₃	**CaO**	**CH₄**
Trace element absent from carbonator model	**Mg**	/		
Trace element absent from calciner model	**Mg**		/	X

Elements/compounds for which data is discontinuous so cannot be used in statistical analysis, but removal of element from the model allows compound/element to be present.
/ Is removal of element from model increases compound presence.
X Is removal of element from model decreases compound presence.
Light grey boxes denote carbonation conditions and element–compound interactions for which there is no effect.
Dark grey boxes denote calcination conditions and element–compound interactions for which there is no effect.
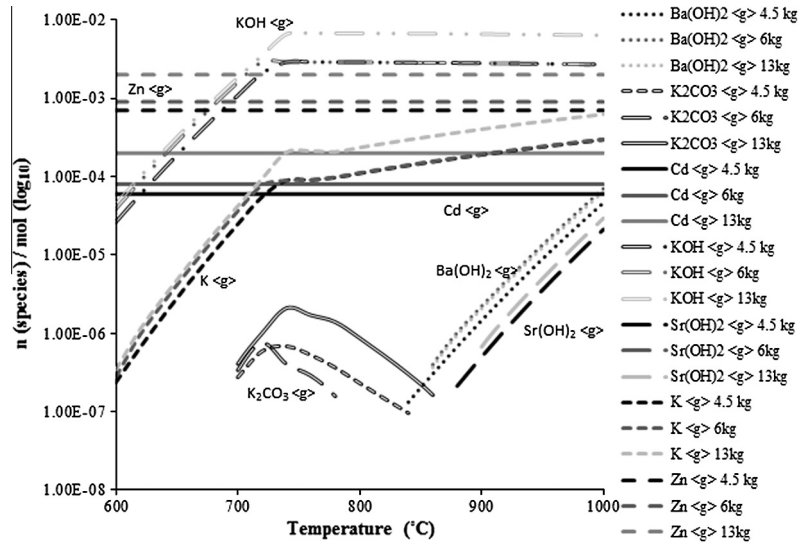
Table 6
MTDATA sensitivity analysis results for 21 elements.

		Compound presence significantly affected by absence of trace element														
		CaCO₃	**CoSb**	**CrLiO₂**	**CaO**	**C**	**CH₄ (g)**	**C₂H₄ (g)**	**H₂ (g)**	**_Pb_**	**_Hg (g)_**	**MnO**	**_Ni_**	**_NiSb_**	**_SrO (g)_**	**_HLiO (g)_**	**_HKO (g)_**
Trace element absent from carbonator model — **Mg**		/			/												
Ni			/														
Al				/													
Trace element absent from calciner model — **Mg**					X	X	X	X	X	/		/	/	/			/
Al							/						/		/		
Sr					/												
Pb							X										
K								/									
V								/									
Se												/					
Cr																/	
Co										/							
Ba										/							

Elements/compounds for which data is discontinuous so cannot be used in statistical analysis, but removal of element from the model allows compound/element to be present.
/ Is removal of element from model increases compound presence.
X Is removal of element from model decreases compound presence.
Light grey boxes denote carbonation conditions and element–compound interactions for which there is no effect.
Dark grey boxes denote calcination conditions and element–compound interactions for which there is no effect.

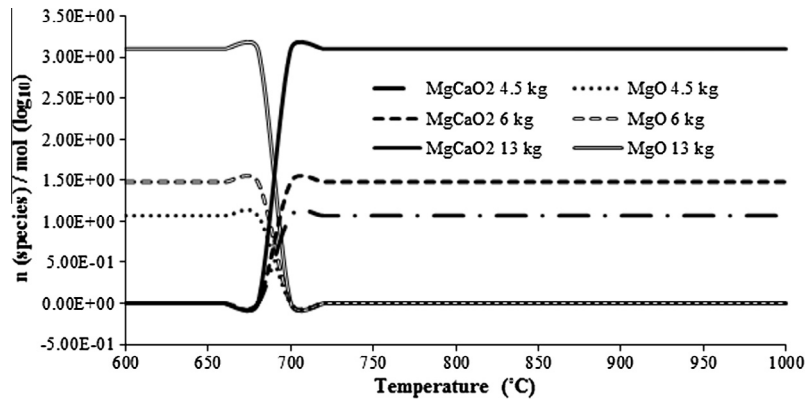**Fig. 14.** Calculated gaseous species (MTDATA) for 4.5 kg, 6 kg and 13 kg sorbent.

Fig. 15. Calculated solid Mg-based species (MTDATA) for 4.5 kg, 6 kg and 13 kg sorbent.
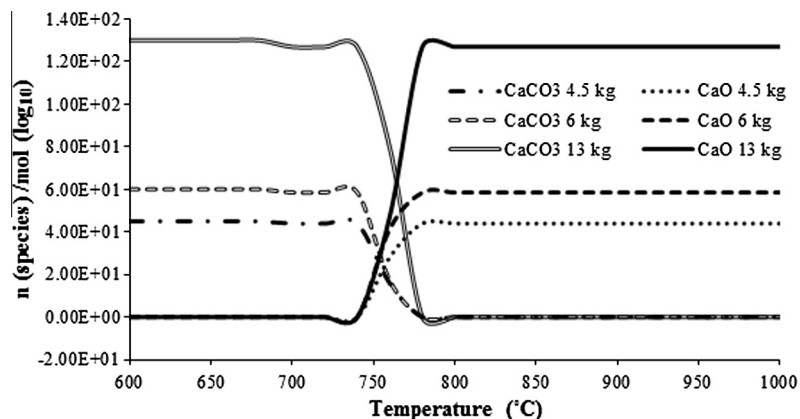

Fig. 16. Calculated solid Ca-based species (MTDATA) for 4.5 kg, 6 kg and 13 kg sorbent.

Mg was identified as one of the primary impurities of limestone (Table 2). Fig. 15 identifies that increasing sorbent mass increases the amount of solid MgO and $MgCaO_2$ at the relevant temperatures at which they are stable, but increasing sorbent mass has no effect on the temperature at which both compounds are stable. Fig. 16 shows a similar trend whereby increasing sorbent mass also increases the mass of solid $CaCO_3$ and CaO present.

3.5. Thermodynamic modelling – effect of SO_2 concentration

It is apparent from the results of MTDATA thermodynamic equilibrium modelling that increasing SO_2 concentration during carbonation has an effect on the species present at equilibrium. Fig. 17 shows that the addition of SO_2 allows the formation of S-based compounds that would not otherwise form if SO_2 was not
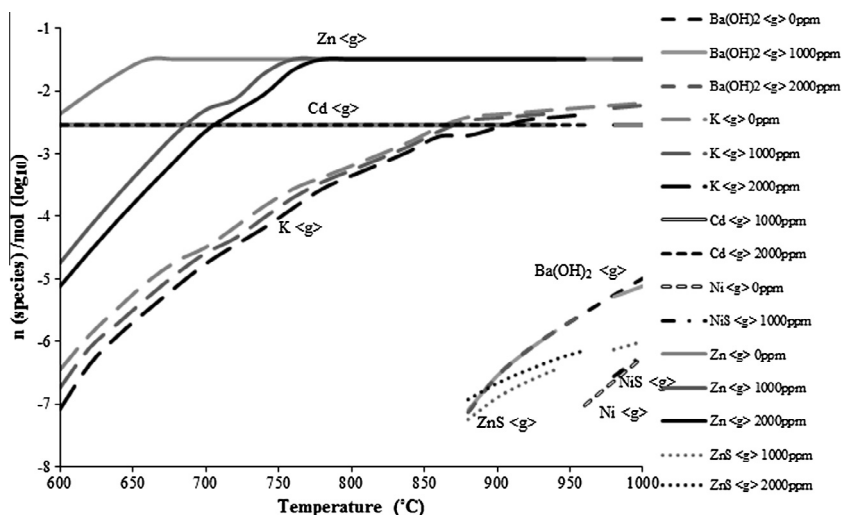
Fig. 17. Calculated gaseous species (MTDATA) for 0 ppm, 1000 ppm and 2000 ppm SO_2.

introduced. For example at 0 ppm SO_2 gaseous Ni and Zn are present, but at 1000 ppm and 2000 ppm SO_2, ZnS is also formed, but only NiS is formed in place of Ni. Experimental data (Fig. 11) identifies a general decrease in Ni concentration with increasing SO_2 concentration, but it would be expected that this would be found as Ni rather than NiS, given the oxidative conditions in the reactor, and the requirement of reducing conditions for H_2S, and in turn NiS formation. Increasing SO_2 concentration appears to have no effect on the stability of gaseous Cd or $Ba(OH)_2$, although experimental data (Fig. 9) confirms a decrease with Ba with increasing SO_2 concentration. SO_2 does appear to have some influence on the stability of gaseous Zn and ZnS, whereby increasing SO_2 concentration appears to reduce the amount of gaseous Zn up until 780 °C, above which temperature the amount of Zn reaches stability at −1.49/mol, regardless of the concentration of SO_2 present. Experimental data (Fig. 10) however confirms decreasing Zn concentration with increasing SO_2 from 0 ppm to 2000 ppm SO_2.Thermodynamic equilibrium data shows there is a small influence on the stability of gaseous K, with increasing SO_2 concentration slightly reducing the amount of gaseous K. For example, at 700 °C and 0 ppm SO_2, calculations show there to be −4.59/mol, compared to −4.75/mol with 2000 ppm SO_2. This however is the opposite of what experimental data (Fig. 10) suggests. Gaseous ZnS formation increases with SO_2 concentration, from −6.9/mol at 900 °C for 1000 ppm SO_2 to −6.7/mol for 2000 ppm SO_2. Again, the predicted formation of sulphides is unexpected given the O_2 concentration in the carbonator (Fig. 4), and highlights the limitations of MTDATA compared to experimental data.

Fig. 18 shows that at approximately 700 °C and with 0 ppm SO_2, the stability of solid MgO decreases, whilst in its place the stability of solid $MgCaO_2$ increases to become the predominant Mg species. Increasing concentrations of SO_2 appear to increase the temperature at which the stability of MgO decreases and the stability of $MgCaO_2$ increases. For example at 2000 ppm, the temperature at which MgO reaches its minimum and $MgCaO_2$ starts increasing is at approximately 740 °C. Fig. 19 shows that increasing SO_2 concentration has minimal effect on the stability of $CaCO_3$ which reaches a minimum at approximately 860 °C, but SO_2 does have a small effect on the stability of CaO, with higher SO_2 concentrations increasing the temperature at which CaO is first formed, from 780 °C with 0 ppm to 820 °C with 2000 ppm SO_2. The model suggests that solid CaS is formed in the presence of SO_2 under conditions typical of

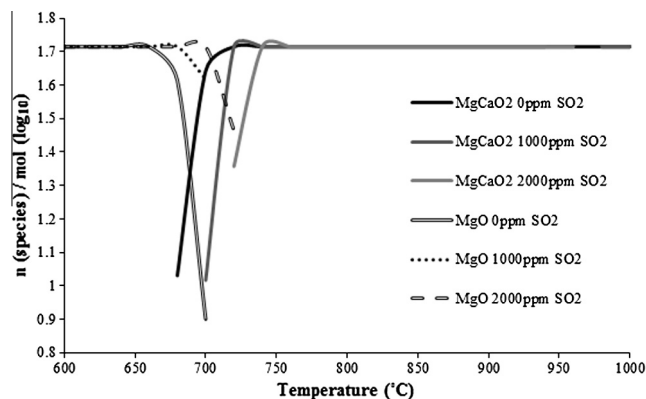**Fig. 18.** Calculated solid Mg-based species (MTDATA) for 0 ppm, 1000 ppm and 2000 ppm SO_2.

carbonation, and higher concentrations of which result in higher amounts of CaS formed.

The results show that thermodynamic modelling is a useful means of supporting experimental data with regards to gaseous trace element compositions and elemental partitioning, over a range of temperature conditions relevant to Ca-based CO_2 capture. However, there may be several reasons for the various discrepancies noted, primarily that MTDATA calculates the reactions at equilibrium, and assumes that the reactions go to completion, when in reality, this may not be the case. In addition, the model databases may not contain all of the compounds relevant to the required experimental conditions, and thermodynamic equilibrium data may not be available for all compounds at all required temperatures. Diffusion rates through sorbent pores are also an important factor in CO_2 capture efficiencies. Work carried out by Bhatia and Perlmutter [36] proposed the 'Random Pore Model' which describes kinetically-controlled fluid–solid reactions, taking into account factors including boundary layers and product layer diffusion. These influences are important when considering experimental reaction rates and in turn efficiencies, but unfortunately are not aspects that can be included when using thermodynamic equilibrium modelling to simulate reactions.
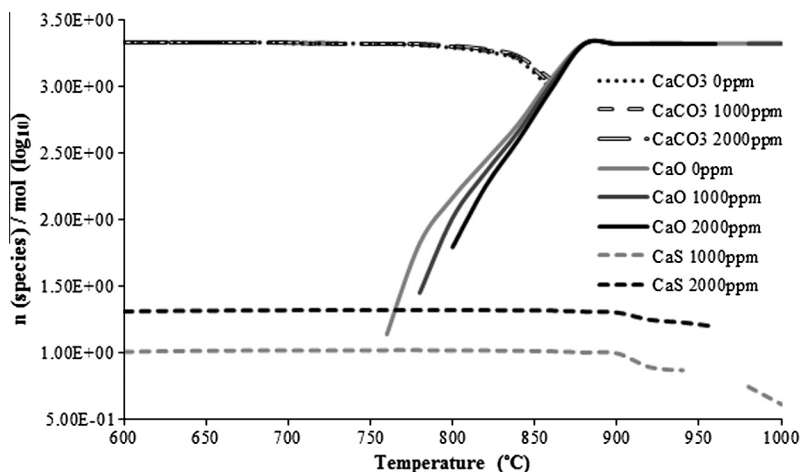
Fig. 19. Calculated solid Ca-based species (MTDATA) for 0 ppm, 1000 ppm and 2000 ppm SO_2.

4. Conclusion

Gaseous element emissions sampling from Cranfield's pilot scale, 25 kWth CO_2 capture reactor using a limestone-derived CO_2 sorbent, was undertaken for a sorbent mass of 4.5 kg, 6 g and 13 kg, and also for SO_2 concentration of 0 ppm, 1000 ppm and 2000 ppm SO_2 in the carbonator reactor. Element emissions to the gaseous phase appeared to be influenced by sorbent mass, with the majority of species increasing in concentration as sorbent mass increased. Increasing SO_2 concentration also appeared to have an effect on gaseous trace element emissions, although the effect appeared to differ depending upon the element concerned, with some increasing in concentration, and other decreasing in concentration as SO_2 concentration increased, suggesting complex underlying chemistry. The mass balances however show that compared to the concentration of elements in the sorbent, the concentrations partitioning to the gaseous phase is very low. Thermodynamic modelling was undertaken to verify the likely elemental speciation and partitioning under CO_2 capture conditions, results of which have proved useful in supporting the experimental work.

The experimental results provide valuable information with regards to scale up of CO_2 capture technology incorporating the Ca-looping cycle, and thermodynamic modelling can be considered a useful instrument in supporting this work, particularly with regards to elemental emissions.

References

[1] Khodier AHM, Hussain T, Simms NJ, Oakey JE, Kilgallon PJ. Deposit formation and emissions from co-firing miscanthus with Daw Mill coal: pilot plant experiments. Fuel 2012;101:53–61.
[2] Oakey JE, Simms N, Kilgallon PJ. Gas turbines: gas cleaning requirements for biomass-fired systems. Mater Res 2004;7(1):17–25.
[3] Bushell AJ, Williamson J. Fate of trace elements in UK coals during gasification processes. Am Chem Soc, Div Fuel Chem 1996;41(3):791–5.
[4] Meij R. Trace element behavior in coal-fired power plants. Fuel Process Technol 1994;39(1–3):199–217.
[5] Trembly JP, Gemmen RS, Bayless DJ. The effect of IGFC warm gas cleanup system conditions on the gas–solid partitioning and form of trace species in coal syngas and their interactions with SOFC anodes. J Power Sources 2007;163(2):986–96.
[6] Córdoba P, Ochoa-Gonzalez R, Font O, Izquierdo M, Querol X, Leiva C, et al. Partitioning of trace inorganic elements in a coal-fired power plant equipped with a wet flue gas desulphurisation system. Fuel 2012;92:145–57.
[7] Font O, Cordoba P, Leiva C, Romeo LM, Bolea I, Guedea I, et al. Fate and abatement of mercury and other trace elements in a coal fluidised bed oxy combustion pilot plant. Fuel 2012;95:272–81.
[8] Sager M. Environmental aspects of trace elements in coal combustion. Toxicol Environ Chem 1999;71(1–2):159–83.
[9] Furimsky E. Characterization of trace element emissions from coal combustion by equilibrium calculations. Fuel Process Technol 2000;63(1):29–44.
[10] Cheng JF, Zeng HC, Zhang ZH, Xu MH. The effects of solid absorbents on the emission of trace elements, SO_2, and NO_x during coal combustion. Int J Energy Res 2001;25(12):1043–52.
[11] González B, Alonso M, Abanades JC. Sorbent attrition in a carbonation/calcination pilot plant for capturing CO_2 from flue gases. Fuel 2010;89(10):2918–24.
[12] Chen H, Zhao C, Chen M, Li Y, Chen X. CO_2 uptake of modified calcium-based sorbents in a pressurized carbonation–calcination looping. Fuel Process Technol 2011;92(5):1144–51.
[13] Barber C. Major and trace element associations in limestones and dolomites. Chem Geol 1974;14(4):273–80.
[14] Dean C. Application of the calcium looping cycle to CO_2 mitigation in the cement process. PhD thesis. Imperial College, London; 2013.
[15] Thompson D, Argent BB. Thermodynamic equilibrium study of trace element mobilisation under pulverised fuel combustion conditions. Fuel 2002;81(3):345–61.
[16] Argent BB, Thompson D. Thermodynamic equilibrium study of trace element mobilisation under air blown gasification conditions. Fuel 2002;81(1):75–89.
[17] Miller BB, Dugwell D, Kandiyoti R. The fate of trace elements during the co-combustion of wood-bark with waste. Energy Fuel 2006;20(2):520–31.
[18] Miller BB, Kandiyote R, Dugwell DR. Trace element behaviour during co-combustion of sewage sludge with polish coal. Energy Fuel 2004;18(4):1093–103.
[19] Kilgallon PJ, Simms NJ, Oakey JE. Fate of trace contaminants from biomass fuels in gasification systems. In: Proceedings of the seventh liege conference, Part I, materials for advanced power engineering; 2002.
[20] Reed GP, Dugwell DR, Kandiyote R. Control of trace elements in a gasifier hot gas filter: a comparison with predictions from a thermodynamic equilibrium model. Energy Fuel 2001;15(6):1480–7.
[21] Goñi C, Helle S, Garcia X, Gordon A, Parra R, Kelm U, et al. Coal blend combustion: fusibility ranking from mineral matter composition. Fuel 2003;82(15–17):2087–95.
[22] Oakey JE, Kara F, Patchigolla K. The effects of impurities for capture technologies on CO_2 compression and transport. In: BCURA Report B93; 2010.
[23] Environmental Protection Agency (EPA) Method 29. Determination of Metal Emissions from Stationary Sources.
[24] Suito K, Namba J, Horikawa T, Taniguchi Y, Sakurai N, Kobayashi M, et al. Phase relations of $CaCO_3$ at high pressure and high temperature. Am Mineral 2001;86(9):997–1002.
[25] So HE. Adsorption of arsenic and phosphate onto the surface of calcite as revealed by batch experiments and surface complexation modelling. PhD thesis. Technical University of Denmark, Denmark; 2011.
[26] Swart P. Trace elements in carbonates (unpublished Short course presentation), University of Miami, US; 2009.
[27] Gitari MW, Petrik LF, Key D, Etchebers O, Okujeni C. Mineralogy and trace element partitioning in coal fly ash/acid mine drainage co-disposed solid residues, 2005 World of Coal Ash (WOCA), April 11–15, Lexington, Kentucky, USA; 2005.
[28] Yan R, Gauthier D, Flamant G. Volatility and chemistry of trace elements in a coal combustor. Fuel 2001;80(15):2217–26.

[29] Bushell AJ, Williamson J. Trace element distributions and associations in UK coals. Fuel Energy Abstr 1996;37(5):332.

[30] Zevenhoven R, Kilpinen P. Trace elements, alkali metals. In: Control of pollutants in flue gases and fuel gases. Finland: Helsinki University of Technology; 2001. p. 8-1–8-30. chapter 8.

[31] Bartonova L, Klika Z. Volatility of Cu, Ni, Cr, Co., Pb and As in fluidised-bed combustion chamber in relation to their modes of occurrence in coal. World Acad Sci, Eng Technol 2009;33:35–8.

[32] Nagarajan R, Madhavaraju J, Nagendra R. (Revista Mexicana de Ciencias Geologicas), geochemistry of neoproterozoic shales of the rabanpalli formation, Bhima Basin, Northern Karnataka, Southern India. Implications for Provenance and Paleoredox Conditions 2007;24(2):150–60.

[33] Berkeley L, Muller G. Raymond Group Research: Luminescant Lanthanide Agents; 2013. Available at: <http://www.cchem.berkeley.edu/knrgrp/ln.html>, (accessed 06.06).

[34] Blamey J, Anthony EJ, Wang J, Fennell PS. The calcium looping cycle for large-scale CO_2 capture. Prog Energy Combust Sci 2010;36(2):260–79.

[35] Miller B, Dugwell DR, Kandiyote R. The influence of injected HCl and SO_2 on the behaviour of trace elements during wood-bark combustion. Energy Fuel 2003;17:1382–91.

[36] Bhatia SK, Perlmutter DD. A random pore model for fluid–solid reactions: II. Diffusion and transport effects. AIChE J 1981;27(2):247–54.